

## Safety systems in magnetically driven wireless capsule endoscopy

M. Salerno, *Student Member, IEEE*, T. Mazzocchi, T. Ranzani, *Student Member, IEEE*, F. Mulana, P. Dario, *Fellow, IEEE*, and A. Menciassi, *Member, IEEE*

**Abstract**— Magnetically driven wireless capsule endoscopy (WCE) represents one of the last achievements in the research of minimally invasive tools for gastrointestinal tract (GI) diagnosis. Recently, capsule localization methodologies have been employed to enable system autonomy maintaining a magnetic link with the device and managing interaction forces with GI tissues. To achieve these objectives, the locomotion platforms exploit automatic motion in some degrees of freedom and unsupervised contact with the external patient abdomen can occur. In this paper safety issues are faced; in particular a safety system, able to monitor pressure with patient abdomen, has been designed, characterized, and integrated with a magnetically driven WCE locomotion platform. New technologies, such as smart textiles, have been employed as sensible element. The proposed system showed promising results in controlling the pressure exerted on the abdomen respecting safety limits and increasing the efficiency and range of locomotion.

### I. INTRODUCTION

Pre-symptomatic detection of gastrointestinal tract (GI) diseases has a very high impact in public welfare. Conventional colonoscopy with flexible endoscopes [1] is currently used for navigating through the GI tract. The main drawbacks of colonoscopes and associated procedures are the limitation in reachable districts and the pain and discomfort that most patients suffer during these examinations, thus limiting their extensive use for screening purposes.

Wireless capsule endoscopes (WCE) may overcome the above issues. High-tech swallowing pills embedding a camera can explore the GI tract by peristalsis and transmit images of anatomical areas unreachable by conventional colonoscopies [2]. Pain and discomfort associated with such technique are considerably reduced but, due to the limited video stream rate and to the difficulty in associating the image acquired with the capsule position, WCE diagnoses are not completely reliable (high number of false negatives) [3]. The possibility to control the capsule position and orientation can improve the current technology by joining the advantages of traditional techniques where the endoscopist has the full control of the camera view point with painless WCE. Many locomotion methods have been designed for WCE [4] [5]; however, it is challenging to find a solution that fits with WCE design constrains (less than 1.5 cm<sup>3</sup> for actuators and battery) [6]. Magnetic dragging of the capsule partially solves these issues; indeed a magnetic coupling between a permanent magnet embedded in the capsule (slave) and an external magnetic field source (master) can be exploited to

move the capsule without energy consumption [7]. However magnetic locomotion methods for WCE have to address a common development step: the localization of the device inside the GI for maintaining a stable magnetic link between the capsule and the external source during the treatment. In [7] [8], a robotic arm is used for holding a permanent magnet thus allowing the medical doctor focus on the visualization of specific areas of interest. A variety of solutions for magnetically driven WCE localization have been investigated in literature [9] [10] [11] [12] and a promising approach is represented by onboard slave device measurements of the master magnetic field source [13] [14] [15]. Although this approach could guarantee the conditions for a reliable locomotion, high accuracy and high localization rate are required to maintain the forces and torques under specific thresholds. This is necessary since magnetic forces suddenly change for small variations of master-slave relative position-orientation, and thus dangerous interaction with GI tract tissues may occur.

These concepts have been introduced by the authors in previous works [16] [17] where a closed control loop exploiting a 2 degrees of freedoms (DoFs) localization method with an accuracy of 2~5 mm and a rate of ~20 Hz has been demonstrated adequate in maintaining the magnetic link with a reliable control on the applied magnetic forces. However, while an automatic closed loop control based on localization feedback provides safe internal interactions between the slave device and the tissues, autonomous motion of the master magnet mounted onto robotic arm can be very dangerous in case of contact with the patient body (Fig. 1). In these circumstances, a safety system supervising contact with patient is mandatory to guarantee safe operating conditions. Furthermore, the possibility to control the contact between the external master magnet and the abdomen during the capsule driving could increase magnetic locomotion effectiveness. Controlling the pressure exerted on the abdomen may allow to apply a controlled force and thus to safely compress the abdomen for reducing the distance between the master and the slave.

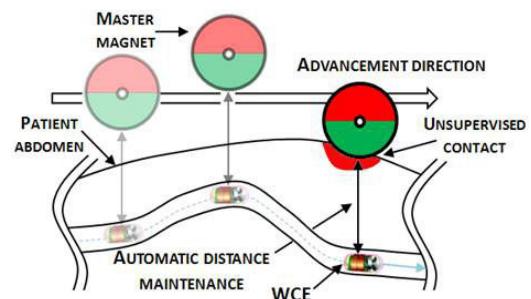


Fig. 1: Example of unsupervised contact with patient abdomen due to anatomy variability and localization based automatic distance maintenance.

\*Research partially supported by the SUPCAM European FP7 project no. 315378 and Fondazione Cassa di Risparmio di Pisa, in the framework of Micro-VAST project

All authors are with The BioRobotics Institute, Scuola Superiore Sant'Anna, Pisa, Italy

M. Salerno is the corresponding author (m.salerno@sss.up.it)

This feature may allow to effectively perform the diagnosis e.g. in over weight patients exploiting a safe compression of the abdomen for moving the capsule. The dynamic tuning of the distance between the moving the capsule and the driving magnet may allow reducing the necessary magnetic forces for the locomotion thus minimizing the size of the inner magnets (embedded in the slave) and improving miniaturization without performance loss. In this paper, a textile pressure sensor has been interfaced with the master magnet and employed as safety system in magnetic WCE as shown in Fig. 2. In order to monitor the pressure generated on patient abdomen, many different solutions can be applied, but textile pressure sensors present some relevant advantages; an analysis of possible sensing solutions applicable to safe magnetically driven WCE is reported in Section II. Sensor choice, design and characterization have been conducted and reported in Section IIIA, the safety system has been tested on a dedicated setup and a closed control loop based on capsule position and contact pressure has been implemented and tested (Section IIIB); finally, experimental results have been reported in Section IV.

## II. CONTACT PRESSURE SENSORS FOR SAFE HUMAN ROBOT INTERACTION

In order to monitor the contact pressures applied from the master device during magnetically driven WCE, a distributed pressure sensor was chosen.

In medical applications, such as tele-echography, a 6 DOFs load cell feedback is employed to maintain a target force on human body [21] [22]. In the presented application, the integration of a load cell interfaced with the robot end-effector has been rejected because, even if forces and torques can be measured with high accuracy, there are three main integration and implementation issues: first, the master magnetic system should be connected with the load cell thus generating a considerable offset and solicitations on the sensing unit that have to be compensated by considering manipulator dynamics; second, the magnetic force applied by the slave device on the master magnetic source will contribute to the measure force/torque, and it could be hard to predict in what measure. Finally, highly concentrated pressures, that are main responsible of discomfort or pain, cannot be evaluated by end-effector load-cells.

Tactile sensing solutions for monitoring robot interaction with the surrounding and with humans have been approached in many different applications, from humanoid robots to assistive robots and manipulators [18]. Different transduction strategies were investigated, such as resistive/piezo-resistive, tunnel effect, capacitive, optical, ultrasonic, magnetic, piezoelectric, etc. [19] [20]. Such sensors have been embedded/interfaced in humanoids, assistive robots and manipulators, for allowing safe contact with humans and leading to sophisticated high level tasks execution. In industrial robotics, impedance control, implemented on multi-degrees of freedom serial robotic arm with torque sensors at each joint, has been employed to guarantee safety and improving maneuverability and human-robot cooperation.

In the presented application, the aim of the safety system is to identify stress concentrations that could result by contacting the patient body. In particular in correspondence of ribs, pelvis or other stiff areas where higher stress

concentrations may be caused during the master driven locomotion. In order to control and avoid such high stress concentrations, the sensing element should map the pressure distribution on the contact area of the tool. Based on these considerations, matrix pressure sensors have been considered for our application.

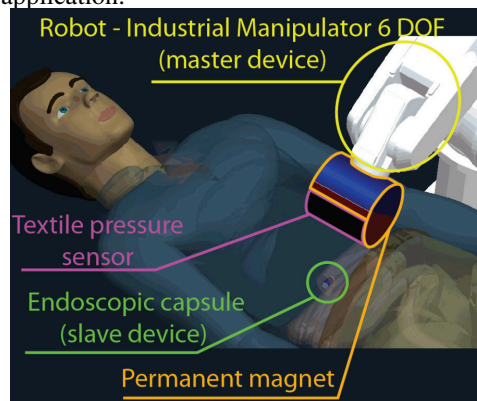


Fig. 2: System overview: the master source is connected to the robot end-effector in order to drive the capsule through the GI tract; the textile pressure sensor is wrapped below the master in order to detect possible contact and forces with patient abdomen.

### A. Available pressure sensors

As regards pressure sensor integration, the sensor thickness should be carefully considered in order not to excessively increase the distance between the driving magnet and the capsule. For this reason a thin sensor with no significant encumbrance should be preferred. A possible arrangement of master, slave and safety system is described in Fig. 2.

There is a variety of off-the-shelf distributed pressure sensors with different working principles and features that could fit the proposed application needs [23].

One of the most widespread solutions is from Tekscan (Tekscan Inc., USA, [www.tekscan.com](http://www.tekscan.com)). These sensors, based on thin layers superimposition, allow obtaining very compact and uniform probes [24]. Unfortunately, customization costs are very high due to the fabrication technique, thus becoming convenient mainly for mass applications.

The main types of commercially available distributed pressure sensors exploit resistive or capacitive effect. Sensors based on the resistance variation of a piezo-resistive layer are more common since they need a rather simple read-out circuitry. Capacitive sensors are based on capacitance variation between two parallel plates when force is applied. Capacitive tactile sensors are generally driven with a high frequency AC signal, thus resulting in a more complicated electronics for signal analysis. Other high performing sensors, based on fiber optics light emission [25] and diffraction evaluation, has been described in [26] but they are currently hard to find on the market.

An interesting class of piezo-resistive pressure sensors is represented by textile sensors [27], whose fabrication technique allows low cost and fast customization/prototyping. In addition, the acquisition system for piezo-resistive based sensors is quite simple and can be designed by employing off-the-shelf components.

In this work, a piezo-resistive textile sensor has been designed and characterized, the reading and power supply

electronics has been assembled and an acquisition system has been set-up.

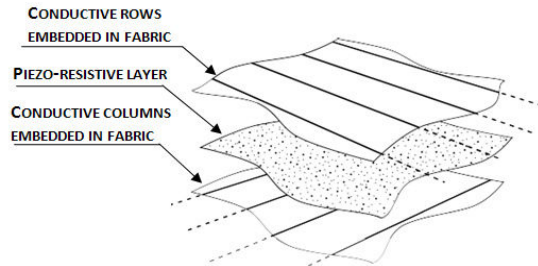


Fig. 3: Flexible matrix textile sensor. The layers composing the sensor allow pressure evaluation due to the intersection of conductive rows and columns embedded in the fabric and distanced by a piezoresistive layer.

### III. MATERIALS AND METHODS

#### A. Pressure sensors calibration

Three different matrix pressure textile sensors provided by Texe (Texe srl, IT, [www.plugandwear.com](http://www.plugandwear.com)) have been characterized. The sensors are composed by two external layers of textiles with a piezo-resistive textile layer interposed as shown in Fig. 3; an additional layer of cotton protects the conductive layer from wear.

The outer layers have conductive rows (copper wire 100  $\mu\text{m}$  in width) and columns knitted in an insulating material (coated copper wire 112  $\mu\text{m}$  in width); consequently the sensitive areas (sensels) are located at each intersection of a row and a column, and the pressure measurement is executed evaluating the resistance at each sensel (Fig. 4).

In order to execute the reading/powering sequence, two multiplexers (ADG732 32:1, Analog Devices, USA) have been interfaced to the sensor rows and columns and an Arduino Mega board (Arduino, ITALY) has been employed to manage the multiplexers (MUX), measure the output voltage and send the voltage data via serial communication. A scheme of powering/reading components is reported in Fig. 5.

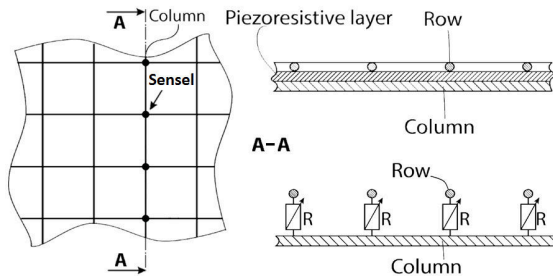


Fig. 4: Flexible matrix textile sensor sensel location description.

The difference between the tested sensors consisted in the piezo-resistive layer employed, EEonTex LG-SL-PA (Eeonyx Co, USA) for high dynamic range (HIGHDYN), EEonTex LR-SL-PA (Eeonyx Co, USA) for low dynamic range (LOWDYN) and Velostat (3M, UK) used as a switch (SWITCH). The size of the sensors is 16 x 16 cm with 8 conductive rows and columns providing 64 sensels. To determine the pressure-resistance relation of the three

different sensors controlled pressures were applied using a loading frame (INSTRON Co, USA). Increasing and decreasing sequences of 30 loads equally spaced between 5 N and 300 N have been applied on a circular area of 2.8  $\text{cm}^2$  corresponding to the area of a single sensel and respective voltages have been recorded. The relation between measured voltage and resistance is described in Eq. 1:

$$R = (V_s - V_{out}) / (V_{out} / R_{pd}) \quad (1)$$

where  $V_s$  is the supply voltage,  $R_{pd}$  is the pull down resistance connected with the ground and  $R$  is the sensel resistance.

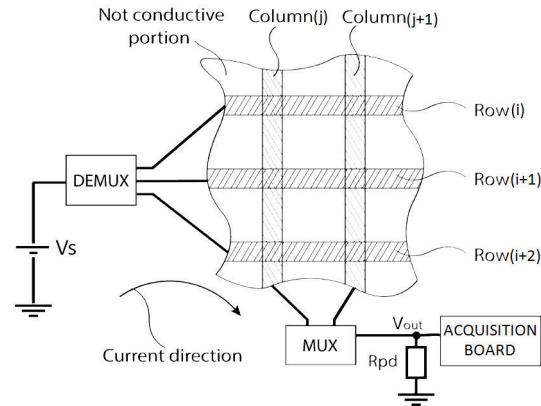


Fig. 5: Powering/reading schema: the sensor powering voltage  $V_s$  is applied to the rows while the sensel resistance is measured through the acquisition board at the columns, the MUX/DEMUX are employed as column/row selectors.

Experimental data resulting from sensors characterization are reported in Fig. 6. Fitting the obtained data the transfer function of eq. 2 was found.

$$P(R) = a R^b + c \quad (2)$$

The experimentally evaluated coefficients  $a$ ,  $b$ ,  $c$  relative to each sensor and the corresponding root mean square error (RMSE) are reported in Table 2. In the case of the SWITCH the maximum pressure is not reported since the behavior is only on/off.

TABLE I.

Sensors features	Tested Sensor		
	HIGHDYN	LOWDYN	SWITCH
a [MPa]	$2.3 \cdot 10^{-7}$	$2.54 \cdot 10^{-8}$	$7.15 \cdot 10^{-16}$
b	-0.758	-1.057	-4.03
c [MPa]	700.6	2043	-1381
RMSE [MPa]	$1.2 \cdot 10^{-3}$	$0.8 \cdot 10^{-3}$	$14 \cdot 10^{-3}$
Maximum detectable pressure [MPa]	~0.1	0.07	~
Minimum detectable pressure [MPa]	$1.8 \cdot 10^{-3}$	$2.3 \cdot 10^{-3}$	$0.2 \cdot 10^{-3}$
Maximum resistance [M $\Omega$ ]	~0.4	~0.4	~
Minimum resistance [M $\Omega$ ]	$0.8 \cdot 10^{-3}$	~	~

Taking into account the characterized sensors calibration curves, the HIGHDYN has been preferred due to its wider pressure range and lower minimum detectable pressure. A pressure of  $\sim 0.3$  MPa has been considered as pressure pain threshold according to [28], where different loads have been applied on subjects' leg providing a feedback on pain. Since the minimum detectable pressure of HIGHDYN is two orders of magnitude lower than the pain threshold, the selected sensor is considered adequate for our safety requirements.

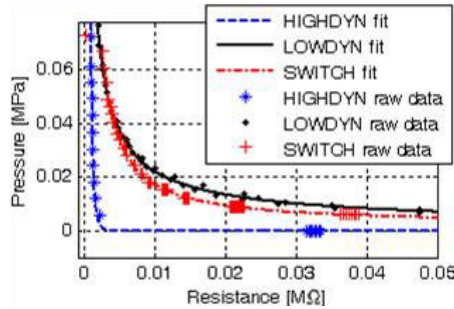


Fig. 6: Calibration curves raw data and fitting.

### B. System development

With the described hardware, the single sensel powering, reading and data communication lasts  $\sim 170\mu\text{s}$ . The localization timing constrains (20 Hz [16], [17]) has been considered in order to design a custom sensor with 256 sensels (resulting in an acquisition rate of  $\sim 22$  Hz) and a sensel distance of 4 mm which is sufficient to identify concentrated pressures. The safety system has been interfaced with the master magnetic source by exploiting a cylindrical frame (Fig. 7a) and the powering/reading electronics has been connected to the robotic unit (Fig. 7b).

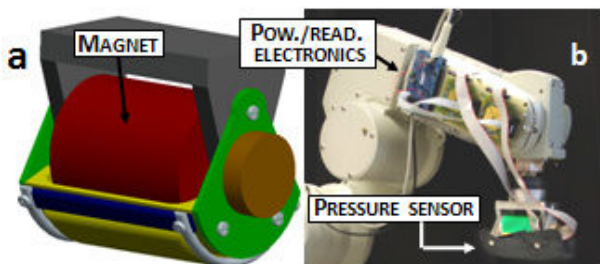


Fig. 7: Cylindrical frame interfaced to the master source (a), pressure sensor and relative electronics interfaced to the robotic unit (b).

The localization module components (including master/slave magnets) are the same employed in previous works [16], [17], but in this case the sensors have been assembled on a custom transceiver board (see Fig. 8), thus increasing acquired data signal/noise ratio and data transmission rate. The prototype has been provided with a battery (3.7 V LiPo cell, LP20 from Plantraco) in order to avoid wirings that could interfere during capsule locomotion. The capsule employed in the tests and described in section IIIC has an outer diameter of 16 mm and a length of 36 mm.

The safety system has been integrated with the closed loop localization based capsule locomotion software (see Fig. 8), providing information about the pressure distributed on the

contact surface. Applied forces and Center of Pressure (COP) coordinates have been selected as input for closed loop control laws.

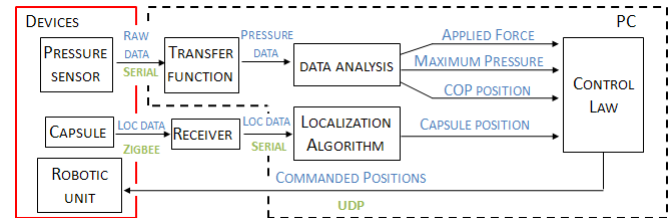


Fig. 8: Hardware and software involved in safe capsule locomotion; data flow in blue, communication methodology in green.

The complete software has been coded in Matlab & Simulink (Matworks, USA) and compiled exploiting the Real Time Windows Target toolbox.

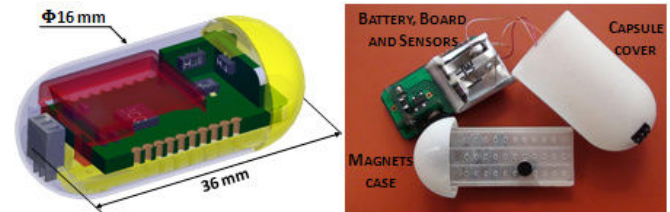


Fig. 9: Capsule endoscope embedding the localization module (top part of the green component), the battery (red component), and the transceiver board (bottom part of the green component). CAD model (left), pre-assembled prototype (right). The magnet case contains four rows of axially magnetized cylindrical magnets

### C. Experimental Tests

A set of tests has been carried out to evaluate safety system performances and to experimentally assess the parameters for a stable control system.

The contact interaction has been considered as a single contact of two convex surfaces (the abdomen and the robot end-effector). Contact interaction with a 3 mm thick Plexiglass sheet, with a curvature radius ranging from 30 cm to 14 cm, has been selected as worst case condition. Indeed, the abdomen generally presents lower curvature and it is less stiff than the plexiglass sheet, thus allowing higher deformations without generating pain in the subject.

Different driving speed ( $V_y$ ) of the master unit along the y axis (Fig. 10a) were tested for simulating the screening procedure. The medical doctor controls the advancement of the capsule while the robot automatically manage the distance along the z axis. The implemented control law aims at maintaining a target force in the direction normal to the contact surface and the orientation of the master magnet moved by the robot, normal to the contact surface (Fig. 10a).

The considered control parameters that influence stability are: a) the speed of the robot approaching the surface ( $V_z$ ) because the robot needs to be able to stop before the maximum allowed force is reached; b) the maximum angular speed of the tool during the alignment of the robotic tool orthogonal to the surface (exploiting the COP location information); c) the horizontal translation speed ( $V_y$ ) since if the speed is too high the contact can be lost. In these tests the system has been considered stable if the contact is maintained without exceeding the pressure limit set at 20% of the 0.3 MPa target pressure (60 kPa).

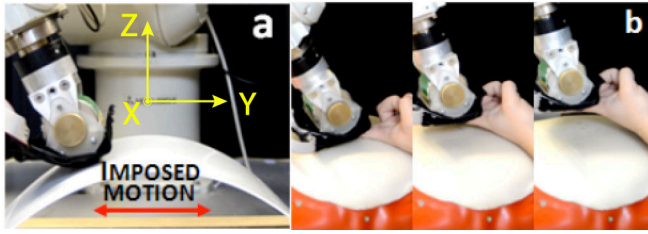


Fig. 10: Force and orientation maintained at target values on plexiglass curved surface (a). Lifting of the robot tool by applying a localized force on the pressure sensor with the fingerr (b).

A qualitative test, involving an abdomen simulator made of a polyethylene net covered with 2 cm of foam rubber and a thin elastic layer, has been performed in order to evaluate the possibility of distancing the robot end-effector from the abdomen manually. Such task could be carried out just interposing a hand between the surfaces in contact and the pressure sensor and manually applying a force on the sensor (Fig. 10b).

A set up reproducing the interaction of the capsule with GI tract tissues and contact of robot end-effector with the abdomen has been developed to evaluate the safe locomotion effectiveness (Fig. 11, left); for more details on the described setup see the companion video.

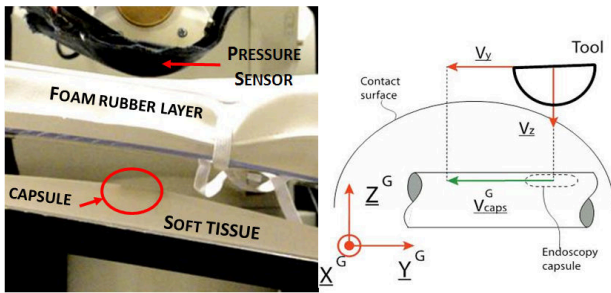


Fig. 11 Set- up employed in safe locomotion tests.

In this test, the control law takes advantage of capsule position and contact pressure feedbacks. The parameters that have been found to guarantee stability in the previous tests have been applied to the control system whenever a contact is detected, giving priority to a safe and painless contact interaction rather than to the capsule distance maintenance. Based on this, the system can automatically stop or generate a warning during the procedure in case capsule magnetic link distance limit is exceeded (i.e. magnetic link close to be compromised) giving to the user the possibility to increment the maximum applicable force and pressure.

#### IV. RESULTS AND DISCUSSION

The tests on curved Plexiglass set-up have been executed at three different horizontal speeds  $V_y$  (10 mm/s, 30 mm/s and 50 mm/s), in Fig. 11, right with a maximum normal to surface advancement speed of 9 mm/s and a maximum angular speed of 30 deg/sec.

Mean maximum and standard deviation of applied force and angular deviation by the normal to the surface direction has been summarized in Table II. In these tests, maximum applied pressures have been evaluated but, since the 60 kPa pressure limit is never overcome, the performance evaluation has been based on force measurements. Keeping constant the other parameters, a horizontal speed of 50 mm/s resulted in

an instable behavior, since pressure maximum error is very high (2,2 N which is 44% of target force) and loss of contact occurs, while with lower speeds the system performs a maximum error of 16%. The angular error shows similar results of error in force; 10 mm/s and 30 mm/s performance can be considered comparable, while at 50 mm/s loss of contact occurred; from this result an upper limit to the possible speed of the diagnostic procedure was found. Fig. 12 shows as an example the force deviation considering the 5 N deformed curved surface as curvilinear abscissa at a horizontal speed of 10 mm/s and 50mm/s. Figure 13 reports as example the resulting trajectories at 10 mm/s and 50 mm/s horizontal speed.

TABLE II.

Evaluated parameters	Horizontal motion speed [mm/s]		
	10	30	50
Mean error in force [N]	0.4	0.2	2.2
Force standard deviation [N]	0,5	0,8	1,5
Maximum error in force [N]	0,8	0,8	1,6
Maximum applied pressure [kPa]	42	46	50
Mean angular error [deg]	1,0	2,8	3,9
Angular standard deviation [deg]	0,9	2,6	4,2
Maximum angular error [deg]	4,4	7,6	12

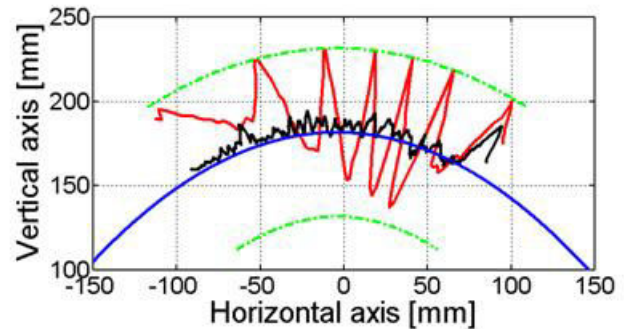


Fig. 12: Force deviation considering the 5 N deformed curved surface as curvilinear abscissa at an horizontal speed of 10 mm/s (black line) and 50 mm/s (red line); the green dashed line represents the lower bound of 10 N.

In joined localization-pressure sensor tests, the translational speed has been set at 30 mm/s in order to maintain stability in case of contact as indicated by the previous results.

In safe locomotion tests, the capsule is constrained by the soft tissue to a trajectory where the thickness of material changes between the capsule and the driving magnet from a lower distance to a higher distance (50 mm range).

Once the contact with the soft tissue is detected the robot speed decreases switching to the previously identified parameters (9 mm/s as maximum speed in surface direction and 30 mm/s maximum horizontal speed) giving priority to the contact management. A graph showing applied force and master-slave distance in case of contact has been reported in Fig.14. For test demonstration and more detailed descriptions refer to the companion video.

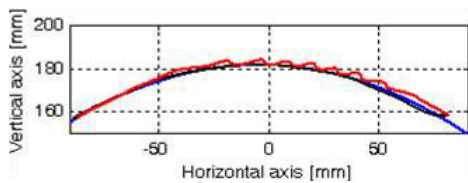


Fig. 13: Robot end effector trajectory at 10 mm/s (black line) and 50 mm/s (red line) horizontal speeds. In blue the theoretical curve if 5 N force, normal to the surface, is applied along the whole surface.

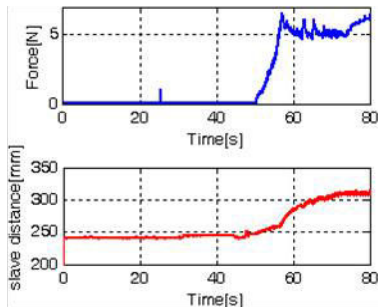


Fig. 14: Force applied on the abdomen (top) and master slave distance (bottom). After the first contact (around 50 s) the system maintains the reference force of 5 N while the master-slave distance increases.

## V. CONCLUSION

In the present paper, the robot-abdomen interaction during WCE magnetic locomotion has been investigated and the possibility of employing textile sensors as safety system has been explored. Textile matrix sensors have been characterized and resulted in a promising solution especially in prototyping and testing phase due to their very fast and low cost customization. The described safety system allows controlling the magnetic link during the magnetic locomotion of the capsule by managing the distance between the capsule and the driving magnet. The integrated pressure sensor demonstrated to allow controlling the pressure exerted on the abdomen in order to increase the efficiency of locomotion and the locomotion range. If the maximum allowed pressure is overcome and the magnetic link is compromised the operator can increase the maximum pressure, if tolerable for the patient, or interrupt the procedure. In the latter case the capsule will be expelled by natural peristalsis. The proposed safety system has been integrated in the capsule locomotion platform both at hardware and software level, showing promising preliminary results. In future work, sensor acquisition rate can be increased employing a more powerful electronics or a set of acquisition boards in parallel configuration; furthermore an extensive system stability analysis considering the joined localization and contact feedback will be carried out.

## VI. REFERENCE

- [1] J. Baillie, "The endoscope" .*Gastrointest Endosc*, vol. 65, 2007, pp. 886-893.
- [2] P. Valdastri, M. Simi, and R.J. Webster III, "Advanced technologies for gastrointestinal endoscopy", *Annu Rev. Biomed Engng*, vol 14, pp 397-429 2012, pp 397-429
- [3] A. Van Gossum, et al "Capsule Endoscopy versus Colonoscopy for the Detection of Polyps and Cancer" *New England Journal of Medicine*, 361, 2009, pp. 264-270
- [4] E. Buselli, P. Valdastri, M. Quirini, A. Menciassi and , P. Dario 2009 "Superelastic leg design optimization for an endoscopic capsule with active locomotion" *Smart Mater. Struct.* 18.12009
- [5] G. Tortora, et al "Propeller-based wireless device for active capsular endoscopy in the gastric district" *Minimally Invasive Therapy & allied technologies*, Vol. 18, No. 5, 2009, pp 280-290.
- [6] X. Wang, M. Q Meng. "Perspective of active capsule endoscope: actuation and localization." *International Journal of Mechatronics and Automation* 1.1 (2011): 38-45.
- [7] G. Ciuti, P. Valdastri, A. Menciassi, P. Dario "Robotic magnetic steering and locomotion of capsule endoscope for diagnostic and surgical endoluminal procedures," *Robotica*, 2010 28, 2010, pp. 199-207.
- [8] G. Ciuti, et al "Robotic versus manual control in magnetic steering of an endoscopic capsule", *Endoscopy*, Vol. 42, 2010, pp. 148-152.
- [9] D. Fischer, R. Schreiber, D. Levi, R. Eliakim, "Capsule endoscopy: the localization system." *Gastrointestinal endoscopy clinics of North America*, 14(1), 25-31, 2004.
- [10] C. Hu, M. Meng, and M. Mandal, "The calibration of 3-axis magnetic sensor array system for tracking wireless capsule endoscope" in *Proc. of the Ieee/RSJ International conference on Intelligent Robots and Systems (IROS2006)*, 2009, pp. 162-167.
- [11] T W R Fountain, P V Kailat J J Abbott, "Wireless control of magnetic helical microrobots using a rotating-permanent-magnet manipulator," *Proc of the IEEE International Conference On Robotics and Automation (ICRA)*, 2010, pp. 576-81.
- [12] C. Di Natali, M. Beccani, P. Valdastri, "Real-Time Pose Detection for Magnetic Medical Devices", *IEEE Transactions on Magnetics*, 2013, 49 (7), 1.
- [13] Y. S. Hong, M. G. Kim, E. J. Lim, "Position and orientation detection of capsule endoscopes in spiral motion," *Int. Precis. Eng. Manuf.* 2009, pp. 31-37.
- [14] M. Salerno, et al "A discrete time localization method for capsule endoscopy based on on-board magnetic sensing," *Meas. Sci. Technol.* 015701, 2012, pp. 10- 23.
- [15] X. Guo, G Yan, W HE, "A novel method of three dimensional localization based on neural network algorithm," *J Med. Eng. Technol.* 33, 2009, pp.192-198.
- [16] M. Salerno F. Mulana, R. Rizzo, A. Landi A. Menciassi, "Magnetic and inertial sensor fusion for the localization of endoluminal diagnostic devices," *Int. J Comput Assist Radiol Surgery (CARS)*, vol 7 no S1, 2012, pp 229-235.
- [17] M. Salerno, R. Rizzo, E. Sinibaldi, A. Menciassi, "Localizzazione and force calculation for magnetic driven capsule endoscopes," *Proc of the IEEE International Conference On Robotics and Automation (ICRA)*, 2013.
- [18] B. D. Argall, A. G. Billard, "A survey of Tactile Human-Robot Interactions," in *Robotics and Autonomous Systems* Vol. 58 , 2012, pp. 1159-1176.
- [19] R.S. Dahiya, G. Metta, M. Valle, G. Sandini, "Tactile Sensing—From Humans to Humanoids," *Robotics, IEEE Transactions on*, vol.26, no.1, 2010, pp.1-20.
- [20] M. R. Cutkosky, R. D. Howe, W. Provancher, "Force and tactile sensors," in *Springer Handbook of Robotics*. B. Siciliano and O. Khatib, Eds. Berlin/Heidelberg, Germany: Springer-Verlag, 2008, pp. 455–476.
- [21] M. Mitsuishi, et al, "Remote ultrasound diagnostic system," *Robotics and Automation*, 2001. *Proceedings 2001 ICRA. IEEE International Conference on*, vol.2, 2001, pp.1567-1574.
- [22] A. Vilchis, J. Troccaz, P. Cinquin, K. Masuda, F. Pellissier, "A new robot architecture for tele-echography," *Robotics and Automation, IEEE Transactions on*, vol.19, no.5, Oct. 2003, pp. 922-926.
- [23] C. M. A. Ashruf, "Thin flexible pressure sensors," *Sensor Review* 22(4), 2002 pp. 322-327.
- [24] T. V. Papakostas, J. Lima, M. Lowe, "A large area force sensor for smart skin applications," In *Sensors, Proceedings of IEEE*, Vol. 2, 2002, pp. 1620-1624.
- [25] E. M. Reimer, L. A Danisch, "Pressure Sensor", W.O. patent 00686, 1998.
- [26] R.S. Dahiya, G. Metta, M. Valle, G. Sandini, "Tactile Sensing—From Humans to Humanoids," *Robotics, IEEE Transactions*, vol.26, no.1, 2010, pp.1-20.
- [27] D. De Rossi, P. Dario, "Composite, multifunctional tactile sensor", U.S. patent:0600738,1984.
- [28] S. Finocchietti, et al "Deformation and pressure propagation in deep tissue during mechanical painful pressure stimulation", *Med. Biol. Eng. Comput.*, 2012, pp. 1-10.